Z. Phys. D 28, 235–245 (1993)

ZEITSCHRIFT
FÜR PHYSIK D

Modified Nilsson model for large sodium clusters

S.M. Reimann[1], **M. Brack**[1], **Klavs Hansen**[2]

[1] Institut für Theoretische Physik, Universität Regensburg, Universitätsstrasse 31, D-93053 Regensburg, Germany
[2] The Niels Bohr Institute, DK-4000 Roskilde, Denmark

Received: 8 March 1993 / Final version: 10 May 1993

Abstract. We propose a modified Nilsson model for spheroidal sodium clusters and investigate the modification of shell structure by deformation for sizes up to $N=850$. For spherical clusters, our potential is fitted to the single-particle spectra obtained from microscopically selfconsistent Kohn-Sham calculations using the jellium model and the local density approximation. Employing Strutinsky's shell-correction method, the surface energy of the jellium model is renormalized to its experimental value. We find good agreement between our theoretically predicted deformed magic numbers and the experimentally observed ones extracted from recent sodium mass abundance spectra.

PACS: 36.40; 35.20.Wg; 71.45.Nt

1. Introduction

The first evidence of shell structure in alkali metal clusters came from experiments of Knight et al. [1, 2]. Enhanced abundances at the "magic numbers" $N=8$, 20, 40, 58, 92... have been shown to correspond to shell closings predicted by spherical jellium model calculations in the framework of density functional theory [3–7]. The dominant peaks in the experimental abundances coincide with the major spherical shell closings expected theoretically. The minor features *between* the major shell closings, however, cannot be understood in a simple spherically symmetric model.

Clemenger [9, 10] was the first to interpret the fine structure of the mass spectra in a particle range $N \leqslant 100$ by spheroidal distortions in a manner analogous to the shape variations of nuclei, using a modified Nilsson Hamiltonian [11] which yields the right splitting of the energy levels due to the loss of spherical symmetry.

In the Nilsson model the potential depends on deformation, and the equilibrium state of each cluster is determined simply by minimizing the sum of the lowest occupied single-particle energies ε_i. Obviously, such a model is far from being self-consistent, as the density distribution of the electrons does not necessarily have the same shape as the potential. Furthermore, the sum of single-particle energies fails to correctly reproduce the total binding energy and to describe the deformation energy surface of an interacting system. These shortcomings tend to become more important as the cluster size increases, and hence a new theoretical approach seems appropriate. Recent measurements of sodium mass distributions of the Copenhagen group [12, 13] make it possible to compare calculated and experimental deformation effects in a large size range.

In the present work, we propose a modified Nilsson potential which in the spherical limit is fitted to the single-particle energy spectrum of Kohn-Sham (KS) calculations within the jellium model. For axially deformed clusters, the potential has the deformation dependence of a spheroidal harmonic oscillator. The total binding energy of a cluster is obtained by use of the Strutinsky shell-correction method [14]. This ensures that the potential energy is not double counted. It furthermore has the advantage that we can renormalize the surface tension to the experimental value.

Our modified Nilsson model represents an approximation to the more involved and time consuming self-consistent calculations for spheroidal shapes [15–17], which up to now were restricted to a particle range $N < 40$. Because of its simplicity, the present model allows an analysis of deformation effects also in very large metal clusters. We find that, indeed, a number of the observed structures in the sodium mass spectra [12, 13] in regions *between* spherically-magic clusters can be understood in terms of static axial deformations, and that there is a good agreement with our predicted deformed-magic numbers.

2. Construction of the model potential

The main idea of our model is to construct a mean-field potential which in the spherical limit closely approxi-

mates that of microscopically selfconsistent KS calculations using the jellium model, but for axially symmetric deformations retains the simplicity of the Nilsson model [11].

We start from the Nilsson Hamiltonian (neglecting the spin-orbit term)

$$\hat{H} = \hat{H}_{\mathrm{HO}} - \hbar\omega_0 \cdot U\mathbf{l}^2 \tag{1}$$

$$\hat{H}_{\mathrm{HO}} = -\frac{\hbar^2}{2M}\Delta + \frac{M}{2}(\omega_x^2 x^2 + \omega_y^2 y^2 + \omega_z^2 z^2), \tag{2}$$

consisting of an anisotropic harmonic oscillator $\hat{H}_{\mathrm{HO}}$ and an $\mathbf{l}^2$-term which splits the degeneracies within the main oscillator shells: for $U > 0$, spherical levels with higher l-values are shifted downwards more than those with smaller l. Thus the $\mathbf{l}^2$-term, depending on the choice of the parameter U, leads to an intermediate situation between a pure oscillator potential and a square well, similar to that of a Woods-Saxon potential.

For spheroids we define the deformation parameter δ through the oscillator frequencies by

$$\omega_x = \omega_y =: \omega_\perp = \omega_0 \mathrm{e}^{\delta/3} \tag{3}$$

$$\omega_z = \omega_0 \mathrm{e}^{-2\delta/3}, \tag{4}$$

so that the ratio q of the semi-axes is

$$q = \frac{\omega_\perp}{\omega_z} = \mathrm{e}^{\delta}. \tag{5}$$

This automatically satisfies the condition of volume conservation

$$\omega_\perp^2 \omega_z = \omega_0^3. \tag{6}$$

So far this model is similar to that of Clemenger. He subtracted, however, a term $\langle \mathbf{l}^2 \rangle_{N_0} = \frac{1}{2} N_0 (N_0 + 3)$ as in later versions of the Nilsson model (see, e.g., [18]), which allowed him to use a *fixed* value of U for the whole spectrum and a certain range of cluster sizes [9, 10].

However, the equilibrium deformations depend rather sensitively on the choice of U, and a priori it is not sure that Clemenger's fit also works well for systems with more than, say, 100 atoms. Therefore, we suggest a procedure which yields a close conformity with spherical KS spectra for all cluster sizes. This correspondence is especially valuable, since recent jellium model KS calculations for very large spherical sodium clusters [6, 7] have yielded excellent agreement with the major shell closings observed experimentally [12, 13].

The starting point for our calculations are the numerically obtained spherical KS levels $\varepsilon_{\mathrm{KS}}$. Our procedure now consists in choosing the value of U such that in the spherical case ($\delta = 0$), the spectrum of the Hamiltonian Eq. (1) reproduces as closely as possible the spectrum $\varepsilon_{\mathrm{KS}}$. This can, of course, only be done with an N dependent value of U. For $\delta = 0$ the eigenvalues are known analytically:

$$\varepsilon(\delta = 0)_{N_0} = \hbar\omega_0 \{N_0 + \tfrac{3}{2} + U \cdot l(l+1)\} \tag{7}$$

with the quantum number $N_0 = 2n_r - 1 + l$ characterizing each oscillator main shell. Plotting the KS levels versus $l(l+1)$, as shown in Fig. 1, we see that the levels belonging to the same value of N_0 lie approximately on straight lines, at least for the lower shells. Thus their l dependence can, indeed, be rather well fitted by the simple Nilsson Hamiltonian Eq. (1), adjusting the slope $\hbar\omega_0 \cdot U$ for each main shell by a simple linear regression procedure. The resulting values of U vary, in fact, only little

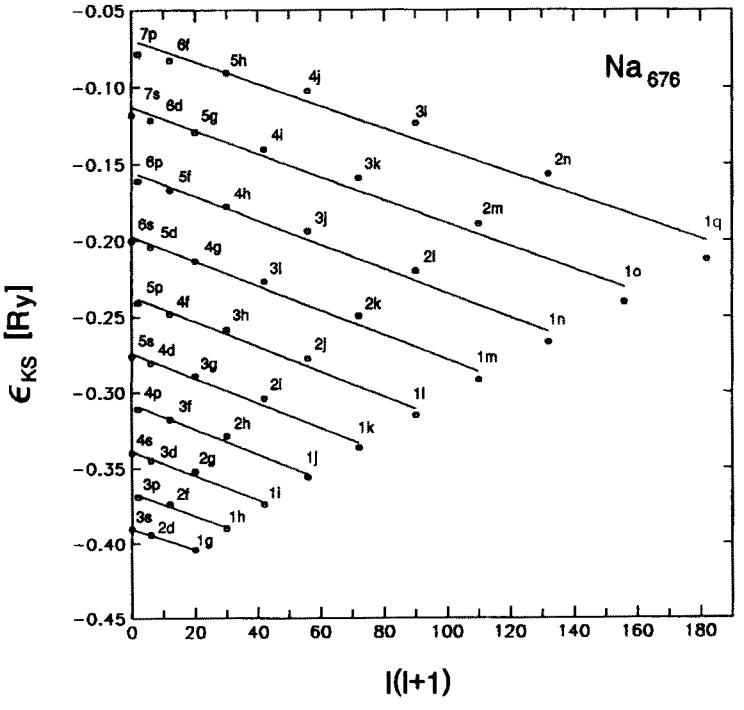

Fig. 1. Spherical Kohn-Sham single-particle energies $\varepsilon_{\mathrm{KS}}$ as functions of $l(l+1)$ for Na_{676}. The corresponding dots in the diagram are labeled with (n_r, l). (We use the nuclear physics convention for the radial quantum numbers n_r). The straight lines indicate the linear-regression fits according to (7)

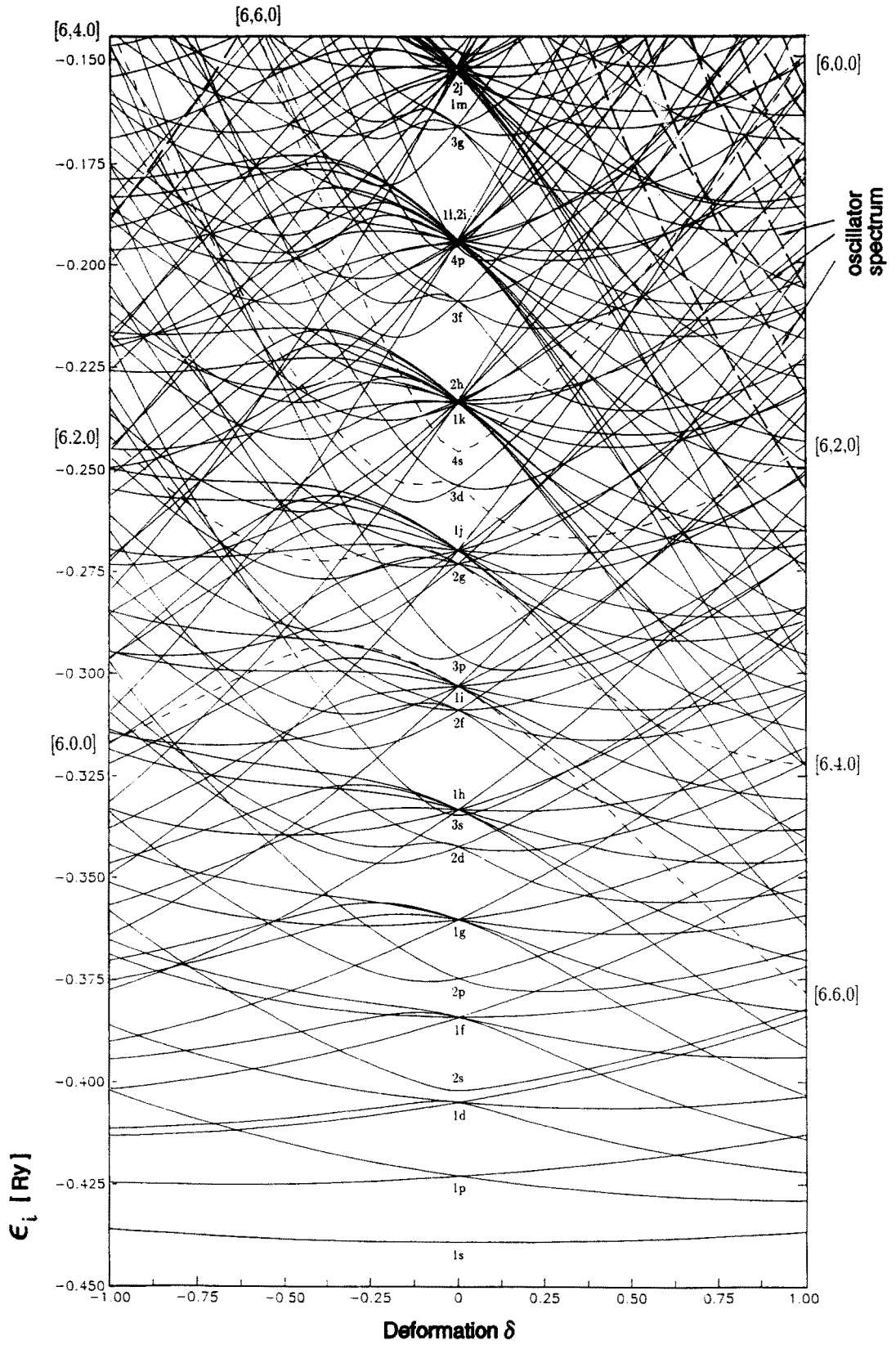

Fig. 2. Single-particle levels of the Nilsson potential as a function of cluster deformation δ for Na_{254}. The dashed lines correspond to states with the asymptotic quantum numbers $[N, n_z, |\Lambda|]$ and show the no-crossing for states with the same symmetry

between the different main shells. For smaller clusters the procedure yields practically the same spherical spectrum as the KS calculations, but for large systems and higher shell numbers N_0, the deviations from straight lines increase. This will lead to an overestimation of the shell effects in the total energy of large clusters, as compared to the results of KS calculations (see, e.g., the peaks at $N=676$ and $N=832$ in Fig. 5a and the discussion at the end of Sect. 4).

The overall energy scale of the potential is determined by the value of $\hbar\omega_0$. In order to adjust it to the scale of the KS spectrum, we relate $\hbar\omega_0$ to the mean square radius $\langle r^2\rangle$. For the isotropic oscillator, the virial theorem yields

$$(\hbar\omega_0)^{(N_0)}=\frac{\hbar^2(N_0+3/2)}{M\langle r^2\rangle_{N_0}}. \tag{8}$$

We use (8) to determine $(\hbar\omega_0)^{(N_0)}$ for each main shell N_0 using the weighted average $\langle r^2\rangle_{N_0}$ given by the KS results.

$\mathbf{l}^2$ is no longer diagonal for $\delta\neq 0$. In the original Nilsson model [11], the basis set of a three-dimensional *isotropic* oscillator was used to calculate the single-particle wave functions and energy eigenvalues. In the limit of large deformations, the eigenvalues are known to correspond to those of the pure *anisotropic* oscillator,

$$\varepsilon_{\mathrm{HO}}(\delta)=(\hbar\omega_0)^{(N_0)}\mathrm{e}^{\delta/3}\{(N_0-n_z+1)+\mathrm{e}^{-\delta}(n_z+\tfrac{1}{2})\}, \tag{9}$$

where $N_0=2n_\perp+|\Lambda|+n_z$, and are characterized by the so-called asymptotic quantum numbers $[N_0,n_z,|\Lambda|]$. In view of this asymptotic behaviour, the expansion of the wave functions in an *anisotropic* harmonic oscillator basis immediately suggests itself, as it has been discussed in [11, 19, 20]. N_0 gives the number of quanta in the corresponding spherical oscillator shell. Λ is the z-component of the angular momentum, while n_z and $n_\perp$ correspond to the nodal numbers of the wave function along the symmetry axis of the spheroid and in a plane perpendicular to it, respectively.

In the asymptotic basis all off-diagonal matrix elements vanish except those differing in $\Delta n_z=\pm 2$ and $\Delta N_0=\pm 2,\ \pm 4$. It has been shown in [20], that making a small change of representation ("stretched coordinates", cf. [11, 20]) is equivalent to neglecting matrix elements between states differing in N_0 and leads to an error of approximately only 1% for deformations in a range $|\delta|\leqq 0.3$.

Due to the axial symmetry, the Hamiltonian is block diagonal, with each block characterized by the parity $\Pi=(-1)^{N_0}$ and the value of $|\Lambda|$. The numerical diagonalization is carried out for the resulting block matrices. Due to the additional selection rule $|\Lambda|\leqq l$, the eigenvalues of each block can be scaled to the KS level with the highest l-value within one oscillator shell N_0. Thus, for $\delta=0$, the Hamiltonian Eq. (1) is now adjusted to approximately reproduce the single-particle spectrum obtained from the KS calculations of [6] for *each* particular cluster size N. The deformation dependence of the single-particle spectrum is then obtained by varying the parameter δ, keeping the values $(\hbar\omega_0)^{(N_0)}$ and U fixed.

In Fig. 2, the eigenvalues are plotted for the cluster Na_{254} as functions of the deformation δ. The dashed lines correspond to the energy levels with the asymptotic quantum numbers $[N,n_z,|\Lambda|]$ specified in the diagram. According to the Neumann-Wigner no-crossing rule [21], levels of the same symmetry may never cross.

For $\delta\neq 0$ the reduced symmetry will partly lift the degeneracy of the spherical spectrum. States differing only in the sign of $|\Lambda|$ will still be four-fold degenerate, while those with $|\Lambda|=0$ are two-fold degenerate, spin degeneracy included.

For large deformations, some of the levels belonging to higher shells are lower in energy than the Fermi surface ε_F. In consequence of the finite depth of the KS potential, the spectra have to be continued with the pure oscillator states (9). As these levels only are important for very large deformations, where they nearly reproduce the asymptotic behaviour of the Nilsson eigenvalues, this gives a reliable approximation.

3. Level densities and cluster stability

The occurrence of shell effects in a bound system of fermions is a consequence of large-scale non-uniformities in the single-particle level density. The levels are typically grouped into bunches or "shells" of degenerate or nearly-degenerate eigenstates. The degree of degeneracy is closely connected to the integrability of the average potential (i.e., the selfconsistent mean field) and its symmetries. Metal clusters with the "magic numbers" 8, 20, (34/40), 58, 92, 138, etc., of valence electrons are examples of systems which have a high stability due to the filling of spherical main shells.

When a spherical shell is only partially filled, the Fermi energy lies in a region of high level density which reduces the stability of the system. In such cases, the system tends to stabilize itself by spontaneously breaking the spherical symmetry – a manifestation of the Jahn-Teller effect [22] – and acquires a deformed equilibrium shape.

The exact quantum-mechanical level density of the discrete energy spectrum ε_i is written as a sum of delta functions:

$$g(\varepsilon)=\sum_i \delta(\varepsilon-\varepsilon_i). \tag{10}$$

Besides a rapidly fluctuating part due to the shell effects, $g(\varepsilon)$ contains also a *smooth* part $g_0(\varepsilon)$, which describes the *average* behaviour of the level distribution. Thus, we may write

$$g(\varepsilon)=g_0(\varepsilon)+\delta g(\varepsilon). \tag{11}$$

The part $\delta g(\varepsilon)$ oscillates with the mean distance between the main shells in the spherical as well as in the deformed spectra.

This is also reflected in the Nilsson diagram (cf. Fig. 2). At certain values of δ, the level density is not uniform as

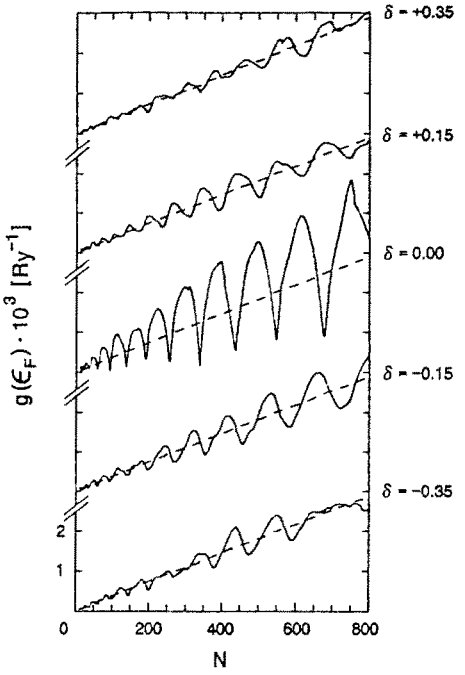

Fig. 3. Level density at the Fermi energy $g(\varepsilon_F)$ (solid lines) and its smooth part $\tilde{g}(\varepsilon_F)$ (dashed lines), plotted as functions of the cluster size N for several values of the deformation parameter δ. The quantity $\delta g(\varepsilon)$ is obtained by folding the spectrum with a gaussian function of width $\gamma = 0.4\,\hbar\omega_0$

a first glance on the eigenspectra suggests, but actually contains large-scale oscillations.

Figure 3 shows the level densities as a function of the cluster size N at the Fermi surface, $g(\varepsilon_F)$, at certain deformations in the Nilsson diagram. (The delta functions of (10) have hereby been replaced by Gaussians with a width of $0.4\,\hbar\omega_0$.) The minima correspond to the more stable configurations. For $\delta = 0$, minima of $g(\varepsilon_F)$ occur at the magic numbers obtained in the KS calculations. But also for $\delta \neq 0$, the level density shows pronounced shell effects, leading to deep minima at particle sizes which do not correspond to any stable configuration with *spherical* symmetry. The shell effects in such deformed systems are less pronounced, due to the partial lifting of the spherical degeneracies. Nevertheless, these deformed shells lead to observable discontinuities, such as the fine structures in the cluster mass yields in the regions $8 < N < 92$ discussed and interpreted by Clemenger [9]. It should be mentioned that in nuclear physics, "magic" nucleon numbers corresponding to deformed shells are well known, in particular in connection with fission; see e.g. [23].

4. Strutinsky's averaging method

In the Nilsson or Clemenger model the total energy of the system is taken to be the sum of the lowest occupied single-particle energies. Obviously, this method fails to reproduce both the absolute binding energies and the relative deformation energies at large deformations. We therefore use a combination of the liquid drop and the shell model, proposed by Strutinsky [14] in the context of nuclear physics. In the following we recall the main points of the Strutinsky method and refer to [14, 23–25] for detailed discussions.

The fluctuations in the level density discussed in the last section lead to variations δE in the total energy, the so-called shell energy correction. Both quantities δE and $\delta g(\varepsilon_F)$ are approximately periodic functions of particle number and deformation, and both have their local minima for the same particle numbers N.

The quantity δE is extracted from the total shell-model energy E_{sh}, which is the sum of occupied levels, by writing

$$E_{\mathrm{sh}} = \sum_{i=1}^{N} \varepsilon_i = \delta E + \tilde{E}. \tag{12}$$

Hereby $\tilde{E}$ is given [14] by

$$\tilde{E} = \int_{-\infty}^{\lambda} \varepsilon \tilde{g}(\varepsilon)\,\mathrm{d}\varepsilon, \tag{13}$$

where $\tilde{g}(\varepsilon)$ is an average level density defined by folding $g(\varepsilon)$ (10) with a smooth distribution function $f_{2M}(x)$, usually taken to be a modified gaussian, over an energy range γ:

$$\tilde{g}(\varepsilon) = \frac{1}{\gamma} \int_{-\infty}^{+\infty} g(\varepsilon') f_{2M}\left(\frac{\varepsilon - \varepsilon'}{\gamma}\right) \mathrm{d}\varepsilon'$$

$$= \frac{1}{\gamma} \sum_i f_{2M}\left(\frac{\varepsilon - \varepsilon_i}{\gamma}\right). \tag{14}$$

The Fermi energy λ is fixed by the equation

$$N = \int_{-\infty}^{\lambda} \tilde{g}(\varepsilon)\,\mathrm{d}\varepsilon. \tag{15}$$

In (14), $f_{2M}(x)$ contains the so-called curvature correction of order $2M$. The purpose of this correction is to guarantee that the smooth part $g_0(\varepsilon)$ in (11) is approximated as closely as possible by the quantity $\tilde{g}(\varepsilon)$. The local value of the level density is reproduced when the folding (14) is applied to a uniform density distribution. Thus, the function $\tilde{g}(\varepsilon)$ is obtained by smearing out the single-particle energies ε_i over an energy range γ which must be of the order $\hbar\omega_0$. $\tilde{g}(\varepsilon)$ therefore does not reflect the existence of shells in the spectrum ε_i, By construction, δE only depends on the levels within a relatively narrow energy interval $\lambda \pm \gamma$ around the Fermi energy, while the contributions from more distant single-particle states cancel.

If the 'true' smooth part $g_0(\varepsilon)$ in (11) is a polynomial of order $2M+1$ in ε, then it is exactly reproduced by $\tilde{g}(\varepsilon)$ in (14). If $g_0(\varepsilon)$ is any analytical function, then $\tilde{g}(\varepsilon)$ approximates it by the first $2M+1$ terms of its Taylor expansion around ε. As discussed in [24], the remaining error may be minimized by imposing on the energy $\tilde{E}$ (13) the stationary condition

$$\left(\frac{\mathrm{d}\tilde{E}}{\mathrm{d}\gamma}\right)_{\gamma=\gamma_0} = 0. \tag{16}$$

Equation (16) is, in fact, the differential form of the usual 'plateau condition' [14] requiring that $\tilde{E}$ does not depend on the averaging width γ in a region $\hbar\omega_0 \lesssim \gamma \ll \lambda$. For the harmonic oscillator, (16) is trivially fulfilled since there $g_0(\varepsilon)$ is a pure second-order polynomial in ε. As a rule, for Nilsson type potentials rather well-pronounced plateaus are obtained, and solutions of (16) can be found with values of the order $\hbar\omega_0 \leqq \gamma_0 \leqq 1.4\,\hbar\omega_0$. This is not surprising, as the smooth level density part of the Nilsson potential is not very different from that of the harmonic oscillator. Varying the order of the curvature correction $2M$ in order to find the best degree of the local polynomial approximation to $g_0(\varepsilon)$, one typically finds $M=3$.

The solution of (16) is found by iteration of γ using a starting value $\gamma \approx \hbar\omega_0$, where the latter corresponds to the average shell spacing at the Fermi surface. The particle conservation (15) has to be fulfilled at each step of the iteration.

Provided that one takes the values of δE at the stationary points γ_0, a third-order curvature correction yields unambiguous results of δE for $N \gtrsim 70$. For light clusters like $N=20$ (cf. Fig. 4a), the plateau condition (16) is not very well established, neither in γ nor in M. Therefore, the use of a *fixed* value of γ_0 may lead to significant uncertainties in the shell correction δE. For small N, the inaccuracy in δE may be as large as 0.010 Ry, but for larger systems, it does not exceed 0.005 Ry for the spherical spectrum $\delta=0$ (cf. Fig. 4b). On the average, these numbers are slightly pushed down for $\delta \neq 0$, as deformation generally tends to make the spectrum more uniform. (For a further discussion of the uncertainties in the averaging procedure, we refer to [26]).

It is the average part of the shell-model energy E_{sh} in (12) which in general has a wrong value. Therefore, the basic idea of Strutinsky [14] is to renormalize $\tilde{E}$ to an empirically determined liquid drop model (LDM) energy which depends smoothly on the cluster size N and deformation δ:

$$E_{\mathrm{tot}}(N,\delta) = E_{\mathrm{LDM}}(N,\delta) + \delta E(N,\delta). \tag{17}$$

Thus, only the fluctuating part δE of the shell-model energy (12) is retained.

The energy E_{LDM} in (17) is taken from the liquid drop model (see, e.g. [27]) which assumes that the particles form a saturated system, having a spatially homogeneous density distribution with a relatively steep surface. In nuclei, the short range of the attractive forces and their repulsive core justify this assumption. In metal clusters, the Coulomb forces have a long range, but due to the positively charged jellium background, the long-range part of the attractive forces is cancelled. As a result, the valence electron system of a metal cluster has a density profile which resembles very much that of an incompressible liquid drop and can be used for a systematic LDM expansion of its average properties [28, 29].

The energy of an incompressible liquid drop is typically written as the sum of three terms proportional to the volume, the surface and the curvature of the system, respectively. Therefore, we write

$$E_{\mathrm{LDM}} = \varepsilon V + \sigma S + \tau C. \tag{18}$$

For monovalent metals the jellium radius R_j is related to the number of valence electrons by

$$R_j = r_s N^{1/3}, \tag{19}$$

where r_s is the Wigner-Seitz radius. Defining the constants $a_v = 4/3\,\pi\varepsilon r_s^3$, $a_s = 4\pi\sigma r_s^2$ and $a_c = 4\pi\tau r_s$, we may

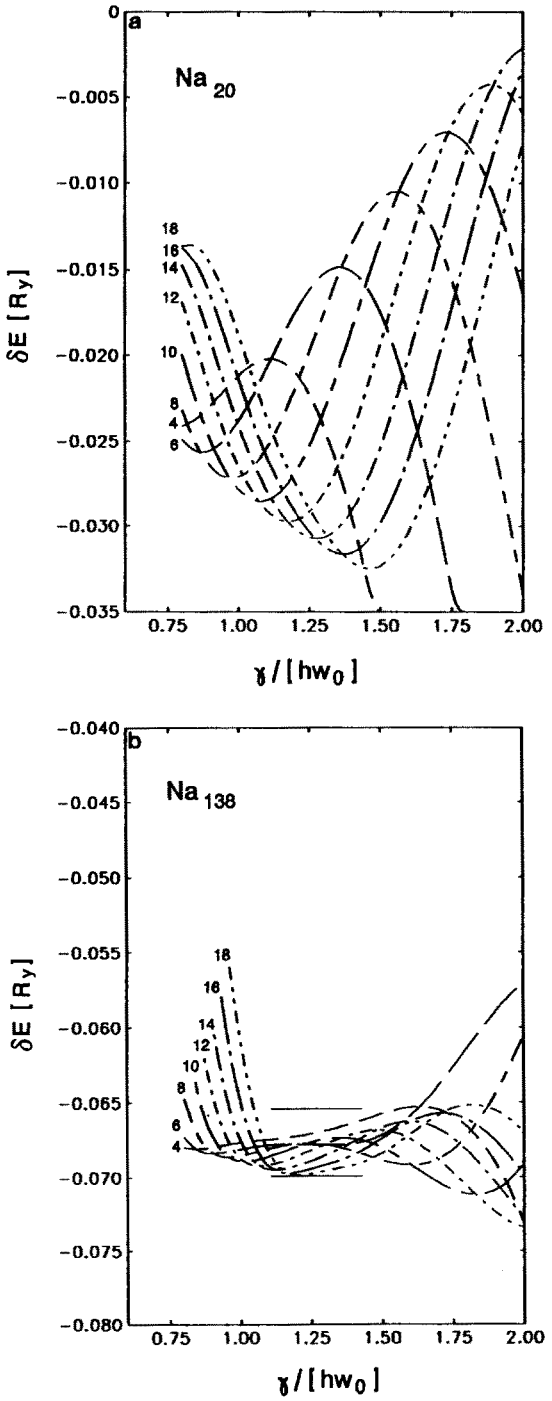

Fig. 4. Dependence of the Strutinsky shell correction δE on the averaging parameter γ for $N=20$ and $N=138$, obtained with correcting polynomials of various degrees $2M$ shown at each curve. An estimate of the inaccuracy in δE for Na_{138} is marked by the solid lines in frame **b**

write, for *spherical shapes*,

$$E_{\mathrm{LDM}}(N,\delta=0)=a_v\cdot N+a_s\cdot N^{2/3}+a_c\cdot N^{1/3}. \tag{20}$$

The parameters a_v, a_s and a_c are the volume (or bulk) energy, the surface energy and the curvature energy, respectively. The deformation energies do not depend on the volume energy, $a_v\cdot N$, as long as the liquid drop is considered to be incompressible.

The jellium model is well-known to give too small surface tensions σ compared to experiment [30]. (For more recent theoretical results of σ or a_s, which all agree within a few percent, see [29].) For sodium, the error is of the order of 20%, and for higher-density metals the situation gets worse: the experimental values increase with decreasing r_s, whereas the jellium results decrease for $r_s<3$ a.u. and even take unphysical negative values (e.g. for aluminum). In order to remedy this situation, we can exploit the advantage of our model where we have a free handle on the LDM parameters. We therefore fixed the surface energy to its experimental value, obtained from extrapolating the measured surface tensions σ of liquid sodium given in [31] to $T=0$ K. This yields $a_s=0.058$ Ry (which is not too different from the melting point value).

The curvature energy was taken to be $a_c=0.052$ Ry, based on the semiclassical calculations of [28]. Other recent theoretical estimates [29] cover a rather wide range of values for sodium, all the way down to $a_c=0.011$ Ry. A recent experimental estimate based on vacancy formation energies [32] gives $a_c=0.024$ Ry. However, we found that for not too small sodium clusters the equilibrium deformations δ_0, and also the shell oscillations in the energies presented below, are fairly insensitive to the choice of a_c in the range mentioned above.

For deformed liquid drops, the surface and curvature terms in (20) have to be multiplied with geometrical coefficients $B_{\mathrm{surf}}(\delta)$ and $B_{\mathrm{curv}}(\delta)$ which contain the deformation dependence (see, e.g., [33] for a tabulation of these coefficients for a variety of shapes and deformation variables). Thus, the final expression for the LDM energy is

$$E_{\mathrm{LDM}}(N,\delta)=a_v\cdot N+a_s\cdot B_{\mathrm{surf}}(\delta)\,N^{2/3}+a_c\cdot B_{\mathrm{curv}}(\delta)\,N^{1/3}. \tag{21}$$

In Fig. 5a, we show the total energy (17) minus its smooth part $E_{\mathrm{LDM}}(N,\delta=0)$ for sodium clusters with up to $N=850$ atoms, evaluated at their equilibrium deformations which are determined by minimizing $E_{\mathrm{tot}}(\delta)$ for each particular cluster size N. The corresponding equilibrium values δ_0 of the deformation parameter are shown in Fig. 5b. In view of the comparison with experiment (see the section below), we have subtracted from the total energy the spherical value of the LDM part which only gives a smoothly varying background as a function of N. The deepest minima in the curve of Fig. 5a correspond

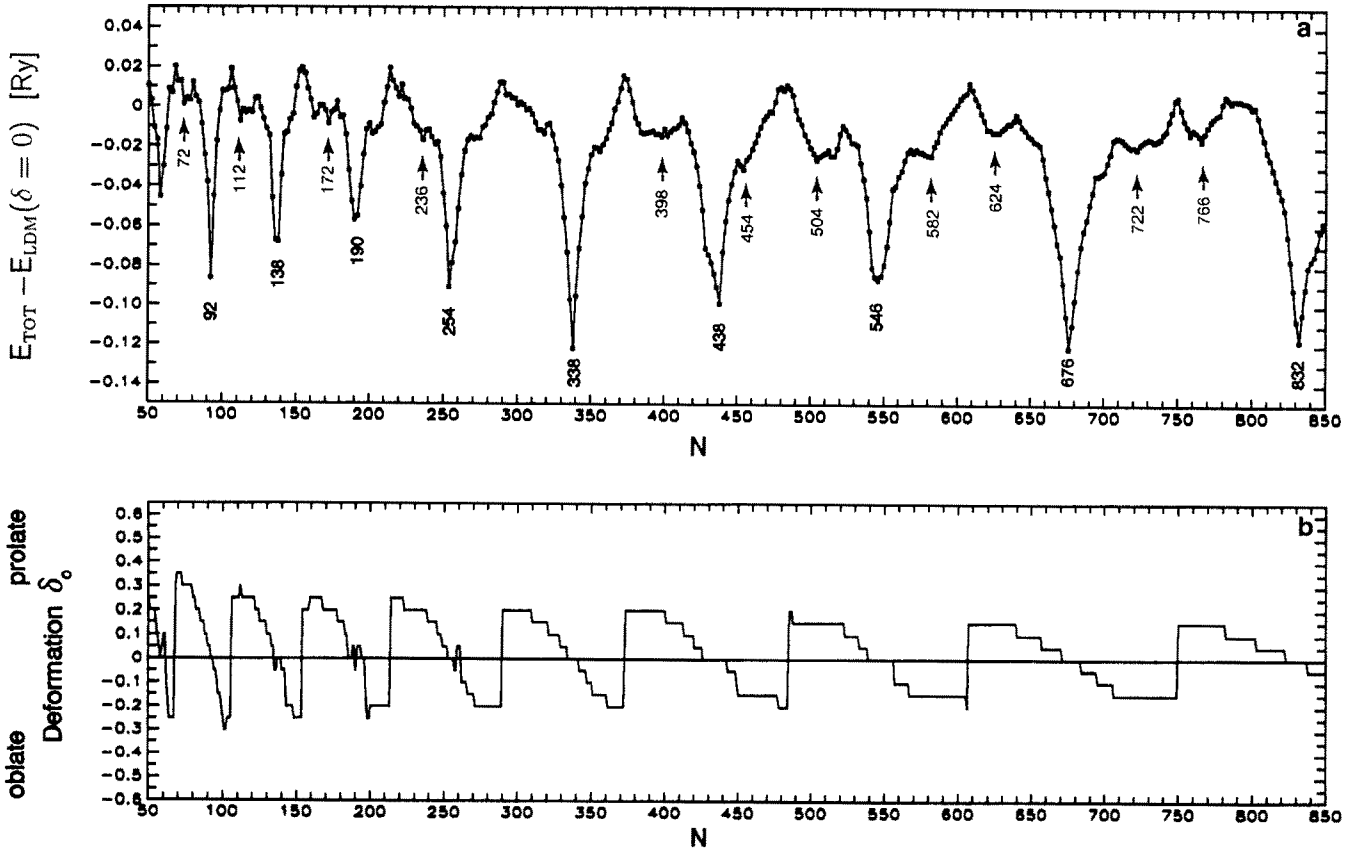

Fig. 5. **a** Total energies minus smooth background, $E_{\mathrm{tot}}(N,\delta_0)-E_{\mathrm{LDM}}(N,\delta=0)$, of sodium clusters versus the atomic number N, evaluated at the corresponding spheroidal ground-state deformations δ_0. **b** Equilibrium deformations δ_0 versus cluster size N on the same scale

to spherical clusters, whereas the smaller minima marked by arrows correspond to axially deformed clusters; the most prominent ones are prolate (see Fig. 5b).

When comparing the fluctuations in the energies of Fig. 5a with those of spherical Kohn-Sham calculations [6, 7, 8], we note that the sharp minima at $N=676$ and $N=832$ are more pronounced in the present results than in the KS results[1]. This has nothing to do with the effects of deformation, since these numbers correspond to spherical clusters, but is simply a consequence of the decreasing quality of our fit of the spherical KS spectrum shown in Fig. 1 for larger N (see the corresponding remark in Sect. 2). Note that the cluster deformations reduce to some extent, but do not abolish, the 'supershell' structure found both in theoretical calculations [6, 34] and in experiment [35]. They reduce the total energies in the regions of deformed clusters - and hereby also smear out some of the fine structure found in spherical calculations due to the filling of subshells - but have no effect near the spherical magic numbers where the shell effects are most pronounced.

5. Comparison with experiment

We now will reanalyze the recently measured cluster mass distributions [12], in order to compare our calculated deformed shell effects to observed structures in the spectra. They represent neutral abundances as produced in a supersonic expansion source and probed by a broad-band UV lamp and a time-of-flight mass spectrometer. (For more details on the experimental procedure, see [12, 13]). The local abundance variations in spectra produced by this type of source are believed to be caused by mainly single-particle evaporation between production and detection. Since the evaporation rate is sensitive to the separation (fragmentation) energy, and this quantity in turn reflects shell structure, the result is an enhancement of the stable clusters.

We have differentiated the experimental spectra using the following generalized logarithmic derivative operation

$$(\Delta_1 \ln I_N)_{K_0} = \frac{\sum_{K=2K_0/3}^{K_0} \frac{2(I_{N+1+K}-I_{N-K})(2K+1)}{(I_{N+1+K}+I_{N-K})}}{\sum_{K=2K_0/3}^{K_0} (2K+1)^2} \quad (22)$$

With this procedure, the statistics in the spectra are artificially improved so that even small variations can be distinguished from statistical fluctuations. In fact, major shell closings now readily appear as negative spikes or, for larger clusters, as broader negative dips. (They will, of course, occur irrespectively of the reason for the local abundance variations.)

Application of the above derivative operation reduces the number of statistically independent data points as compared to the raw spectrum. The density of data points depends on the parameter K_0, and the value chosen thus represents a compromise between improved statistics and the highest observable frequency modulation of the spectrum. By fine tuning K_0, it is then possible to gain information on intermediate frequency oscillations in the abundance spectra.

The data from different runs have been analysed in the way described above, and a carefully determined smooth background was subtracted. The sum of these are shown in Fig. 6 with the values of K_0 indicated. The following broad, low amplitude dips are reproducible between the major shell closings:

$N=66(5)$, 80(10), 116(15), 170(25), 240(20), 390(15), 640(20).

The widths given in parentheses are estimates based on a visual inspection of the plotted logarithmic derivatives. It is our experience that these widths are rather insensitive to the value of K_0 in the range used here. Thus they are expected to be a fair representation of the actual widths, independent of the numerical development used here.

Some of the dips in Fig. 6 have already been seen previously without any fine tuning of K_0 [12, 13, 35]. The peak at $N=640$ is the only case where a peak, previously thought to be a single spherical shell closing, splits into two.

The theoretically expected dip at $N=504/516$ which, in fact, shows a rather prominent structure in δE, cannot be identified in the experimental spectra.

It should be noted that here we are comparing the derivatives of the experimental mass abundances directly with the calculated zero-temperature energies in Fig. 5a, rather than with the second derivatives of the total free energy F as done recently with fully selfconsistent Kohn-Sham results [6–8]. Our reason for not doing so here is that our present δE as a function of particle number, due to the plateau uncertainties in the Strutinsky averaging, contains small high-frequency fluctuations to which the second (or even the first) derivatives are very sensitive [36]. These fluctuations are expected to be strongly damped when a finite temperature of the electrons is included [8]. However, the extension of the Strutinsky method to finite temperatures, though formally possible (see, e.g., [25]), is numerically involved and would lead beyond the scope of our present simple model - the more so since also the temperature dependence of the LDM parameters is uncertain.

Alternatively, one could compare the theoretical results with the *integrated* logarithms of the experimental abundances. These should be proportional to the oscillating part of the total energy (whose average part has been subtracted with the smooth background). We have, however, chosen not to compare these integrated abun-

[1] We cannot compare our total energies to selfconsistent KS energies due to our use of the empirical LDM parameter a_s which is different to the jellium-KS value, and our fit of the spherical KS spectrum which is only approximate

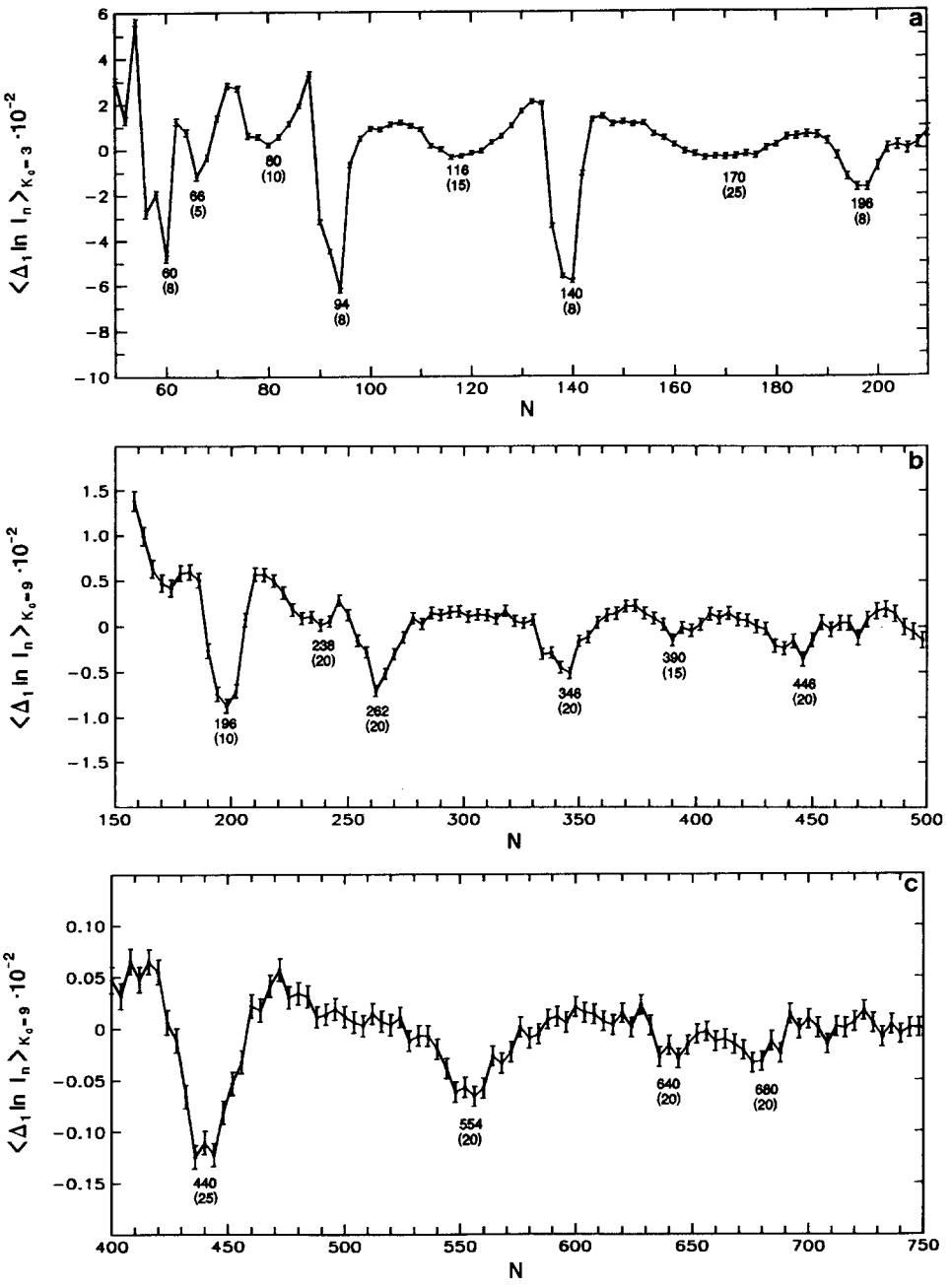

Fig. 6. The logarithmic derivatives according to (22) of experimental mass abundances for sodium clusters [12]. The values of K_0 used are 3, 9 and 9 for frame **a**, **b** and **c**, respectively. In the first two frames, the background has been subtracted in the spectra used. In frame **c** the background is included to avoid uncertainties relating to the background subtraction. Comparison of amplitudes in different frames is thus not possible. Each frame includes at least three different spectra

dances to the theoretical results, because the amplitude of its oscillations is strongly suppressed as compared to the somewhat idealized theoretical zero-temperature calculation, resulting in rather weak signatures. It is clear from the data, however, that the *positions* of the spherical as well as the deformed shell closings in the derivative and integrated spectra are consistent, at least for $N < 500$. This non-trivial fact allows us to draw conclusions based on the derivative spectrum which displays deformation much more clearly.

Our calculations cannot at present be expected to give a good measure of the observed amplitudes or the shapes of the shell oscillations in the mass yields. The clarification of these relations is the subject of current work [37]. We furthermore note that the deformation dips seem to be shifted by a small but systematic amount towards higher particle numbers when compared to the theoretical results. Whether this is a real shift in position or due to the comparison with shell-correction energies as opposed to second derivatives, is not possible to say. However, the shift is small and does not invalidate the general agreement between theoretical and experimental positions of the deformed shells.

6. Conclusions

In summary, we have found a good agreement between the calculated and the observed positions for shells of deformed equilibrium shapes for large sodium clusters. In our theoretical curves we see more fine structure than in the experimental data. From the experimental side, this

is partly due to the averaging procedure used and partly an effect of the finite temperature, which is inherent in the type of source used. The finite temperature will tend to wash out the relatively weak effects both by thermal electronic excitations, and by ionic shape fluctuations. We do, however, observe that the dips that are expected theoretically to be strong tend to survive, with the exception of the region $504 \leqq N \leqq 516$. In addition, we would like to mention the possibility that both improved statistics and alternative experimental procedures could resolve substructures in the peaks observed with the present method [12, 13]. Possibly threshold ionization could also be used as a probe in this connection. Actually, recent measurements of the shell dependent chemical reactivity of large sodium clusters [38] also show a minor shell structure between the spherical shell closings.

Very recently, mass abundance spectra of lithium and sodium clusters by Bréchignac et al. [39] have also revealed some structures between the most prominent spherical magic numbers. Since only total yields were given in [39], the comparison with our results is difficult; in particular, for $N > 400$ the structures in the total yields are too weak to allow for a significant comparison. However, those structures which can clearly be seen for sodium at $N = 70$, 114, ~ 290 and 375 are in good agreement with our deformed shells indicated in Fig. 5a. Perhaps, the subtraction of a smooth background and a differentiation might make it possible to give a more detailed comparison of these data with our results and also with the Copenhagen data shown in Fig. 6.

On the theoretical side, the restriction to axially symmetric shapes of mainly quadrupole nature represents a limitation of our model which leads to an overestimation of the amplitude of the shell effects. As recently shown by Hamamoto et al. [40], nonaxial shapes of both quadrupole and octupole multipolarity can be expected to play a role, in particular in the mid-shell regions between the major spherical systems. The inclusion especially of nonaxial deformations is expected to further wash out the oscillations in δE due to their breaking of the angular momentum (Λ) degeneracy.

While this paper was under preparation, we became aware of a recent study by Frauendorf and Pashkevich who used the Strutinsky method with a phenomenological potential of Woods-Saxon type [34] for sodium clusters with $N \leqq 300$, including axial octupole and hexadecapole deformations [41] and, in an extension, higher-order deformations up to multipolarity $l = 6$ [42]. In spite of the differences of the two models, their results are very similar. The minimization with respect to deformations with $l > 2$ leads to a further reduction of the shell oscillations in their results, but the positions of the most prominent dips corresponding to prolate-deformed shells agree quantitatively with ours.

Helpful discussions with S. Bjørnholm, S. Frauendorf, O. Genzken and Th. Hirschmann are gratefully acknowledged. We would like to thank O. Genzken for putting his Kohn-Sham jellium code at our disposal. One of us (S.M.R.) would like to thank the Studienstiftung des deutschen Volkes for support. This work has also been partially supported by the Danish Natural Science Foundation, Deutsche Forschungsgemeinschaft and the Commission of the European Communities.

References

1. Knight, W.D., Clemenger, K., de Heer, W.A., Saunders, W.A., Chou, M.Y., Cohen, M.L.: Phys. Rev. Lett. **52**, 2141 (1984)
2. Knight, W.D., de Heer, W.A., Clemenger, K., Saunders, W.A.: Solid State Commun. **53**, 445 (1985)
3. Ekardt, W.: Phys. Rev. **B29**, 1558 (1984)
4. Beck, D.E.: Solid State Commun. **49**, 381 (1984)
5. Chou, M.Y., Cleland, A., Cohen, M.L.: Solid State Commun. **52**, 645 (1984)
6. Genzken, O., Brack, M.: Phys. Rev. Lett. **67**, 3286 (1991)
7. Genzken, O.: Ph.D. Thesis, Regensburg 1992 (unpublished)
8. Brack, M., Genzken, O., Hansen, K.: Z. Phys. D**21**, 65 (1991); ibid **19**, 51 (1991)
9. Clemenger, K.: Phys. Rev. **B32**, 1359 (1985)
10. Clemenger, K.: Ph. D. Thesis, Berkeley 1985 (unpublished)
11. Nilsson, S.G.: K. Dan. Vidensk. Selsk. Mat. Fys. Medd. **29**, 16 (1955)
12. Bjørnholm, S., Borggreen, J., Echt, O., Hansen, K., Pedersen, J., Rasmussen, H.D.: Phys. Rev. Lett. **65**, 1627 (1990)
13. Bjørnholm, S., Broggreen, J., Echt, O., Hansen, K., Pedersen, J., Rasmussen, H.D.: Z. Phys. D**19**, 47 (1991)
14. Strutinsky, V.M.: Sov. J. Nucl. Phys. **3**, 449 (1967); Nucl. Phys. A**95**, 420 (1967); ibid A**122**, 1 (1968)
15. Ekardt, W., Penzar, Z.: Phys. Rev. **B38**, 4273 (1988)
16. Lauritsch, G., Reinhard, P.-G., Meyer, J., Brack, M.: Phys. Lett. A**160**, 179 (1991)
17. Hirschmann, Th.: Diploma Thesis, Universität Regensburg 1991 (unpublished); Hirschmann, Th., Brack, M.: (to be published)
18. Lamm, I.L.: Nucl. Phys. A**125**, 504 (1969)
19. Rassey, A.J.: Phys. Rev. **109**, 949 (1957)
20. Brack, M.: Diploma Thesis, Universität Basel 1968 (unpublished)
21. Neumann, J.V., Wigner, E.P.: Z. Phys. **30**, 427 (1929)
22. Jahn, H.A., Teller, E.: Proc. R. Soc. (London) Ser. A**161**, 220 (1937)
23. Brack, M., Damgaard, J., Jensen, A.S., Pauli, H.-C., Strutinsky, V.M., Wong, C.Y.: Rev. Mod. Phys. **44**, 320 (1971)
24. Brack, M., Pauli, H.-C.: Nucl. Phys. A**207**, 401 (1973)
25. Brack, M.: In: Workshop on nuclear models. Oak Ridge 1992. Bengtsson, R. et al. (eds.), p. 345. New York: Wiley 1993
26. Sobiczewski, A., Gyurkovich, A., Brack, M.: Nucl. Phys. A**289**, 346 (1977)
27. Bethe, H.A., Bacher, R.F.: Rev. Mod. Phys. **8**, 82 (1936)
28. Seidl, M.: Diploma Thesis, Universität Regensburg 1989 (unpublished)
29. Brack, M.: Phys. Rev. B **39**, 3533 (1989); Seidl, M., Spina, M.E., Brack, M.: Z. Phys. D**19**, 101 (1991); Engel, E., Perdew, J.P.: Phys. Rev. B**43**, 1331 (1991); Fiolhais, C., Perdew, J.P.,: Phys. Rev. B**45**, 6207 (1992); Makov, G., Nitzan, A.: Phys. Rev. B**47**, 2301 (1993)
30. Lang, N.D., Kohn, W.: Phys. Rev. **B1**, 4555 (1970)
31. Germer, D., Mayer, H.: Z. Phys. **210**, 391 (1968)
32. Perdew, J.P.: Wang, Y., Engel, E.: Phys. Rev. Lett. **66**, 508 (1991)
33. Hasse, R.W., Myers, W.D.: Geometrical relationships of macroscopic nuclear physics. Springer Series in Nuclear and Particle Physics. Berlin, Heidelberg, New York: Springer 1988
34. Nishioka, H., Hansen, K., Mottelson, B.R.: Phys. Rev. **B42**, 9377 (1990)
35. Pedersen, J., Bjørnholm, S., Borggreen, J., Hansen, K., Martin, T.P., Rasmussen, H.D.: Nature **353**, 733 (1991)
36. Reimann, S.M.: Diploma Thesis, Universität Regensburg 1992 (unpublished)

37. Hansen, K., Nishioka, H., Døssing, T., Bjørnholm, S.: (in preparation)
38. Lange, T., Gröhlich, H., Näher, U., Martin, T.P.: Ber. Bunsenges. Phys. Chem. **96**, No. 9 (1992)
39. Bréchignac, C., Cahuzac, Ph., Carlier, F., Frutos, M. de, Roux, J.Ph.: Phys. Rev. B**47**, 2271 (1993)
40. Hamamoto, I., Mottelson, B.R., Xie, H., Zhang, X.Z.: Z. Phys. D**21**, 163 (1991)
41. Frauendorf, S., Pashkevich, V.V.: Z. Phys. D**26**, 98 (1993)
42. Frauendorf, S.: Private communication; Frauendorf, S., Pashkevich, V.V. (to be published)
43. Balian, R., Bloch, C.: Ann. Phys. **63**, 592 (1971); ibid. **69**, 76 (1972)
44. Strutinsky, V.M., Magner, A.G., Ofengenden, S.R., Døssing, T.: Z. Phys. A**283**, 269 (1977)
45. Reimann, S.M., Brack, M.: Comp. Mat. Sci. (Proceedings TAMC1, Leer 1993) (submitted)

Note added in proof. Following the ideas of Balian and Bloch [43] and Strutinsky et al. [44], we have recently shown [45] that the average negative slopes of the equilibrium deformations δ_0 versus N, as displayed in Fig. 5b, can be interpreted in terms of classical periodic orbits. For a spheroidal cavity, Strutinsky et al. [44] found that the main contributors to the gross-shell structure are the rhomboidal orbits in the planes containing the symmetry axis. In the equatorial plane, the leading closed orbits are regular polygons; they are only important for strong prolate deformations.